Organic Electronics 9 (2008) 557–568

Contents lists available at ScienceDirect

Organic Electronics

journal homepage: www.elsevier.com/locate/orgel

Green phosphorescent iridium dendrimers containing dendronized benzoimidazole-based ligands for OLEDs

Wei-Sheng Huang [a], Jiann T. Lin [b,*], Hong-Cheu Lin [a,*]

[a] Department of Materials Science and Engineering, National Chiao Tung University, Hsinchu, Taiwan, ROC
[b] Institute of Chemistry, Academia Sinica, Taipei, Taiwan, ROC

ARTICLE INFO

Article history:
Received 2 January 2008
Received in revised form 19 February 2008
Accepted 1 March 2008
Available online 18 March 2008

PACS:
85.60.Jb
73.61.Ph
72.80.Le

Keywords:
Iridium complexes
Dendrimers
Phosphorescence
Light-emitting diodes

ABSTRACT

A series of novel non-conjugated functionalized benzoimidazole-based dendrimers containing peripheral benzyl ether type dendrons have been synthesized and characterized. These compounds undergo cyclometalation with iridium trichloride to form iridium(III) complexes. The emission wavelengths of these dendrimers are in the range from 510 to 530 nm, and the photoluminescence quantum yields (PLQYs) in the range from 0.45 to 0.80. Dendrimers (**G*n***)$_2$**Ir**(**acac**) and (**G*n***)$_3$**Ir** exhibit a reversible one-electron oxidation wave at ~0.55 V and ~0.37 V (vs. Ag/$AgNO_3$), respectively. With a device configuration of indium tin oxide/poly(3,4-ethylenedioxythiophene):poly(styrene sulfonic acid)/4,4′-bis(*N*-carbarzolyl)biphenyl:(**G2**)$_3$**Ir** 20 wt% dopant/1,3,5-tris(2-*N*-phenyl-benzoimidazolyl)benzene/LiF/Al has a maximum external quantum efficiency (EQE) of 17.6% and a maximum current efficiency of 61.5 cd/A.

1. Introduction

Organic light-emitting diodes (OLEDs) have attracted considerable interests after Tang [1] and Burroughes's [2] report on organic (small molecule) and polymer LEDs (PLEDs). The quantum mechanical constraint sets an upper limit of the internal quantum efficiency at 25% on the fluorescence-based devices. The seminal work by Thompson demonstrated that electroluminescent devices based on heavy transition-metal complexes had great potentials to achieve an internal quantum efficiency of 100% [3]. In these complexes, both singlet and triplet excitons can contribute to emission due to efficient spin-orbit coupling which removes the spin selection regulation during radiative relaxation of the excited state. Several high performance OLEDs based on phosphorescent transition-metal complexes, including Ir [4], Pt [5], Os [6], and other metals [7], have been reported in recent years.

Small organic molecules are usually vacuum deposited for device fabrication, and the facilitation of carrier injection as well as the balance of carrier mobility can be achieved in multi-layer devices. In comparison, spin-coating technique has to be used for PLEDs due to low volatility of polymers [8]. Normally, multi-layer devices are not possible for PLEDs due to difficulty in finding appropriate solvents for casting different layers. However, spin-coating technique renders PLEDs with flexible substrates or large area displays viable. Dendrimers of appropriate molecular weights are considered to be substitutes for polymers, since they may possess similar electronic property and/or morphology as their polymer counterparts. Compared to polymers, it is relatively easy to control the molecular weights of the dendrimers precisely. Consequently,

* Corresponding authors. Tel.: +886 2 27898522; fax: +886 2 27831237 (J.T. Lin); tel.: +886 3 5712121x55305; fax: +886 3 5724727 (H.-C. Lin).
E-mail addresses: jtlin@chem.sinica.edu.tw (J.T. Lin), linhc@cc.nctu.edu.tw (H.-C. Lin).

1566-1199/$ - see front matter © 2008 Elsevier B.V. All rights reserved.
doi:10.1016/j.orgel.2008.03.001

researches on dendrimer light-emitting diodes (DLEDs) have steadily progressed in recent years.

A lot of solution processed DLEDs based on fluorescent dendrimers have been reported [9]. However, these devices only exhibit low efficiencies in most cases. In order to improve the efficiency of DLEDs, phosphorescent metal complexes encapsulated with dendrons are potential candidates. In this regard, Burn and co-workers developed a series of dendritic iridium complexes which emitted in red, green, and blue regions. The electroluminescent (EL) devices using these complexes as dopants in various hosts were reported to have good efficiencies, for example, a maximum external quantum efficiency (EQE) of 5.7% at 80 cd/m^2 for a red light-emitting device [10a], a maximum current efficiency of 55 cd/A at 400 cd/m^2 for a green light-emitting device [10b], a maximum EQE of 8.1% at 3450 cd/m^2 for a green light-emitting device [10c], and a maximum EQE of 10.4% at 100 cd/m^2 for a blue light-emitting device [10d]. Some solution processed host-free DLEDs were also reported by Burn to have high maximum EQE values around 13.6% [11]. Wang reported green-emitting phosphorescent iridium dendrimers with benzoimidazole-based ligands containing carbazolyl dendrons. The dendrimers were fabricated as high-quality films, and thus a highly efficient host-free device with a maximum EQE of 13% and a maximum luminous efficiency of 34.7 cd/A was achieved. By doping the dendrimers into a host of *N*-(4-([9,3′; 6′,9″]tercarbazo-9′-yl)phenyl)carbarzole (TCCz), the maximum EQE can be further increased to 16.6% [12].

Previously, a series of highly phosphorescent cyclometalated iridium complexes containing benzoimidazole-based ligands have been developed [13]. These complexes emit light ranging from green to red, and EL devices using these materials exhibit excellent efficiencies. In this report, we extended our study to dendrimers so as to fabricate solution-processable DLEDs. Non-conjugated Fréchet-type dendrons are used to prevent the iridium-emitting cores from changing their chroma. Green-emitting bis- and tris-cyclometalated complexes based on 1,2-diphenyl-1*H*-benzoimidazole ligands are investigated, and up to the third-generation of dendrimers have been synthesized. DLED devices based on these dendrimers are also explored.

2. Experimental

2.1. Characterization

^{1}H NMR spectra were recorded on a Bruker AMX400 spectrometer. FAB-mass spectra were collected on a JMS-700 double focusing mass spectrometer (JEOL, Tokyo, Japan) with a resolution of 3000 for low resolution and 8000 for high resolution (5% valley definition). For FAB-mass spectra, the source accelerating voltage was operated at 10 kV with a Xe gun, using 3-nitrobenzyl alcohol as the matrix. MALDI-mass spectra were collected on a Voyager DE-PRO (Applied Biosystem, Houston, USA) equipped with a nitrogen laser (337 nm) and operated in the delayed extraction reflector mode. Elemental analyses were performed on a Perkin-Elmer 2400 CHN analyzer. Cyclic voltammetry experiments were performed with a CHI-621B electrochemical analyzer. All measurements were carried out at room temperature with a conventional three-electrode configuration consisting of a platinum working electrode, an auxiliary electrode, and a nonaqueous $Ag/AgNO_3$ reference electrode. The $E_{1/2}$ values were determined as $1/2(E_p^a + E_p^c)$, where E_p^a and E_p^c are the anodic and cathodic peak potentials, respectively. The solvent used was CH_2Cl_2 and the supporting electrolyte was 0.1 M tetrabutylammonium hexafluorophosphate. Electronic absorption spectra were obtained on a Cary 50 Probe UV–visible spectrometer. Emission spectra were recorded in deoxygenated solutions at 298 K by a JASCO FP-6500 fluorescence spectrometer. The emission spectra were collected on samples with o.d. ~0.1 at the excitation wavelength. UV–visible spectra were checked before and after irradiation to monitor any possible sample degradation. Emission maxima were reproducible within 2 nm. The solution luminescence quantum yields (Φ_{PL}) were calculated relative to **Ir(ppy)**$_3$ (Φ_{PL} = 0.40 in toluene) [14]. The solid film quantum yields were measured with an integrating sphere under an excitation wavelength of 350 nm on a quartz glass. All luminescence quantum yields were taken as the average of three separate determinations and were reproducible within 10%. Luminescence lifetimes were determined on an Edinburgh FL920 time-correlated pulsed single-photon-counting instrument. Samples were degassed via freeze–thaw–pump cycle at least three times prior to measurements. Samples were excited at 337 nm from a nitrogen pulsed flashlamp with 1 ns FWHM pulse duration transmitted through a Czerny–Turner design monochromator. The solution emission was detected at 90° via a second Czerny–Turner design monochromator onto a thermoelectrically cooled red-sensitive photomultipler tube. The resulting photon counts were stored on a microprocessor-based multichannel analyzer. The instrument response function was profiled using a scatter solution and subsequently deconvoluted from the emission data to yield an undisturbed decay. Nonlinear least squares fitting of the decay curves were performed with the Levenburg–Marquardt algorithm and implemented by the Edinburgh Instruments F900 software. The reported values represent the average of at least three readings. Atomic force microscopic analyses were carried out by using a Digital Instruments Multimode III atomic force microscope. Images were captured by tapping mode with a silicon tip at a frequency of 300 kHz. For transmission electron microscopy (TEM) studies, the measurements were performed at room temperature (298 K) using a 200 kV electron microscope (JEOL JEM-2100).

2.2. Device fabrication

A layer of poly-(3,4-ethylenedioxythiophene) (PEDOT) doped with poly(styrenesulfonic acid) (PSS) with 70 nm thick was spin-coated on pre-cleaned ITO-coated glass substrates as a hole injection layer and then baked at 100 °C in air for 1 h. Then, a layer of iridium dendrimers doped into poly-(9-vinylcarbazole) (PVK, with thicknesses of ~25, ~40, and ~50 nm for **G1**–**G3**-based complexes, respectively), or 4,4′-bis(*N*-carbarzolyl)biphenyl (CBP, with thicknesses of ~30, ~45, and ~70 nm for **G1**–**G3**-based complexes, respectively) as emitters was spin-coated at a

spin rate of 3000 rpm (revolution per minute) using dichloroethane as the solvent (concentration: 10 mg mL^{-1} for the host and *x* wt% iridium dendrimer as the guest). Then the electron transporting properties of DLEDs, a layer (with a thickness of 40 nm) of 1,3,5-tris(*N*-phenylbenzimidazol-2-yl)benzene (TPBI) was vacuum deposited. Finally, a layer of LiF/Al (1 nm/ 120 nm) cathode was thermally evaporated as a cathode in a vacuum chamber (under a pressure of less than 2.5×10^{-5} torr).

3. Materials

Chemicals and solvents were reagent grades and purchased from Aldrich, Acros, TCI, and Lancaster Chemical Co. Solvents were dried by standard procedures. All reactions and manipulations were carried out under N_2 with the use of standard inert atmosphere and Schlenk techniques. All column chromatography was performed by using silica gel (230–400 mesh, Macherey-Nagel GmbH & Co.) as the stationary phase in a column which is 25–35 cm in length and 2.5 cm in diameter.

3.1. 2-(Phenol-4yl)-1-phenyl-1H-benzoimidazole

N-Phenyl-*o*-phenylenediamine (9.21 g, 50 mmol) and 4-hydroxybenzaldehyde (6.10 g, 50 mmol) were dissolved in 40 mL of 2-methoxyethanol. The mixture was heated to reflux for 48 h under N_2 atmosphere. After cooling, the reaction was quenched with water and the mixture was washed with CH_2Cl_2. The solid was then collected by filtration and pumped dry to give the desired product (5.1 g, 35%). ^{1}H NMR ($CDCl_3$, 400 MHz, ppm): δ 7.71 (d, J = 8.0 Hz, 1H), 7.57–7.51 (m, 3H), 7.36 (d, J = 8.0 Hz, 2H), 7.32 (d, J = 8.4 Hz, 2H), 7.26 (t, J = 7.2 Hz, 1H), 7.20 (t, J = 7.2 Hz, 1H), 7.11 (d, J = 8.0 Hz, 1H), 6.68 (d, J = 8.4 Hz, 2H). FABMS: m/z 287.2 ($(M+H)^+$). Anal. Calcd. for $C_{19}H_{14}N_2O$: C, 79.70; H, 4.93; N, 9.78. Found: C, 79.29; H, 5.04; N, 9.58.

3.2. General procedures for the syntheses of dendritic ligands ***Gn*** (***n*** = ***1***–***3***)

2-(Phenol-4-yl)-1-phenyl-1*H*-benzoimidazole (0.73 g, 2.5 mmol), K_2CO_3(0.35 g, 2.5 mmol), and 1.0 equiv. of various generations of **D*n*** (***n*** = **1**–**3**) were dissolved in 20 mL of dimethylformamide. The mixture was heated at 100 °C for 24 h. After cooling, the reaction was quenched by water and the mixture was extracted with CH_2Cl_2. The combined extract was then washed with brine, dried over $MgSO_4$, and evaporated to dryness. The crude product was purified by column chromatography (silica gel) using a mixture of CH_2Cl_2 and *n*-hexane (1:1 by volume) as the eluent.

G1: White solid. Yield = 87%. ^{1}H NMR ($CDCl_3$, 400 MHz, ppm): δ 7.96 (d, J = 8.0 Hz, 1H), 7.57 (d, J = 8.8 Hz, 2H), 7.54–7.52 (m, 3H), 7.39–7.26 (m, 8H), 7.20 (d, J = 8.0 Hz, 2H), 6.90 (d, J = 8.8 Hz, 2H), 5.04 (s, 2H). FABMS: m/z 377.2 ($(M+H)^+$). Anal. Calcd. for $C_{26}H_{20}N_2O$: C, 82.95; H, 5.35; N, 7.44. Found: C, 82.69; H, 5.40; N, 7.72.

G2: White solid. Yield = 87%. ^{1}H NMR ($CDCl_3$, 400 MHz, ppm): δ 7.86 (d, J = 8.0 Hz, 1H), 7.50–7.45 (m, 5H), 7.39–7.27 (m, 13H), 7.20 (d, J = 8.0 Hz, 2H), 6.85 (d, J = 8.8 Hz, 2H), 6.62 (d, J = 2.0 Hz, 2H), 6.55 (t, J = 2.0 Hz, 1H), 5.06 (s, 4H), 4.96 (s, 2H). FABMS: m/z 589.2 ($(M+H)^+$). Anal. Calcd. for $C_{40}H_{32}N_2O_3$: C, 81.61; H, 5.48; N, 4.76. Found: C, 81.46; H, 5.38; N, 4.74.

G3: White solid. Yield = 70%. ^{1}H NMR ($CDCl_3$, 400 MHz, ppm): δ 7.94 (d, J = 8.0 Hz, 1H), 7.54 (d, J = 8.8 Hz, 2H), 7.51–7.43 (m, 3H), 7.43–7.29 (m, 23H), 7.19 (d, J = 8.0 Hz, 2H), 6.87 (d, J = 8.8 Hz, 2H), 6.64 (d, J = 2.0 Hz, 4H), 6.60 (d, J = 2.0 Hz, 2H), 6.58 (t, J = 2.0 Hz, 2H), 6.52 (t, J = 2.0 Hz, 1H), 5.09 (s, 2H), 5.04 (s, 8H), 4.91 (s, 4H). FABMS: m/z 1013.6 ($(M+H)^+$). Anal. Calcd. for $C_{68}H_{56}N_2O_7$: C, 80.61; H 5.57; N, 2.76. Found: C, 80.42; H, 5.44; N, 2.87.

3.3. General procedures for the syntheses of iridium dendrimers (***Gn***)$_2$***Ir***(***acac***) (***n*** = ***1***–***3***)

To a flask containing $IrCl_3 \cdot nH_2O$ (176 mg, 0.5 mmol) and 1.0 equiv. of various generations of ligands, ***Gn***, a 3:1 mixture of 2-ethoxyethanol and water (25 mL) was added. The mixture was then refluxed for 48 h and cooled to room temperature. After cooling, the reaction was quenched by water and the mixture was washed with CH_2Cl_2. The solid formed was collected by filtration and pumped dry to give the crude product of the μ-chloro-bridged Ir(III) dimer. This crude product was mixed with Na_2CO_3 (0.30 g, 3.0 mmol), 2,4-pentanedione (0.30 g, 3.0 mmol), and 2-methoxyethanol (20 mL) in a flask. The mixture was heated to reflux for 24 h. After cooling, the reaction was quenched by water and the mixture was extracted with CH_2Cl_2. The combined extract was then washed with brine, dried over $MgSO_4$, and evaporated to dryness. The crude product was isolated by column chromatography on a silica gel column using a mixture of CH_2Cl_2 and *n*-hexane (1:1 by volume) as the eluent.

(**G1**)$_2$**Ir**(**acac**): Yellow solid. Yield = 80%. ^{1}H NMR ($CDCl_3$, 400 MHz, ppm): δ 7.67–7.59 (m, 12H), 7.49–7.45 (m, 2H), 7.25–7.20 (m, 10H), 7.18–7.08 (m, 4H), 6.79 (d, J = 8.0 Hz, 2H), 6.13–6.04 (m, 4H), 5.22 (s, 1H), 4.59 (d, J = 12.0 Hz, 2H), 4.56 (d, J = 12.0 Hz, 2H), 1.84 (s, 6H). FABMS: m/z 1042.3 (M^+). Anal. Calcd. for $C_{57}H_{45}N_4O_4Ir$: C, 65.69; H, 4.35; N, 5.38. Found: C, 65.43; H, 4.56; N, 5.51.

(**G2**)$_2$**Ir**(**acac**): Yellow solid. Yield = 55%. ^{1}H NMR ($CDCl_3$, 400 MHz, ppm): δ 7.67–7.56 (m, 12H), 7.51–7.49 (m, 2H), 7.40–7.29 (m, 20H), 7.22–7.15 (m, 3H), 7.02 (d, J = 8.0 Hz, 2H), 6.49–6.47 (m, 2H), 6.43–6.42 (m, 2H), 6.38 (d, J = 1.6 Hz, 3H), 6.20–6.07 (m, 4H), 5.22 (s, 1H), 4.88 (s, 8H), 4.51 (s, 4H), 1.84 (s, 6H). FABMS: m/z 1466.8 (M^+). Anal. Calcd. for $C_{85}H_{69}N_4O_8Ir$: C, 69.61; H, 4.74; N, 3.82. Found: C, 69.13; H, 4.92; N, 3.53.

(**G3**)$_2$**Ir**(**acac**): Yellow solid. Yield = 20%. ^{1}H NMR ($CDCl_3$, 400 MHz, ppm): δ 7.64–7.50 (m, 2H), 7.56–7.52 (m, 4H), 7.50–7.43 (m, 4H), 7.34–7.28 (m, 40H), 7.07–7.01 (m, 4H), 6.58 (d, J = 8.0 Hz, 8H), 6.52 (s, 8H), 6.47–6.37 (m, 6H), 6.24–6.20 (m, 2H), 6.08–6.02 (m, 4H), 5.21 (s, 1H), 4.99–4.93 (s, 16H), 4.81–4.77 (m, 12H), 1.84 (s, 6H). FABMS: m/z 2314.8 (M^+) Anal. Calcd. for $C_{141}H_{117}N_4O_{16}Ir$: C, 73.13; H, 5.09; N, 2.42. Found: C 72.84, H 5.00, N 2.30.

3.4. General procedures for the syntheses of iridium dendrimers (***Gn***)$_3$***Ir*** (***n*** = ***1***–***3***)

One equiv. of μ-chloro-bridged Ir(III) dimer was mixed with K_2CO_3(2.5 equiv.), ***Gn*** (2.0 equiv.), and glycerol

(5.0 mL) in a flask. The mixture was heated at 190 °C for 24 h. After cooling, the reaction was quenched by water and the mixture was extracted with CH_2Cl_2. The combined extract was then washed with brine, dried over $MgSO_4$, filtered, and evaporated to dryness. The crude product was isolated by column chromatography on a silica gel column using a mixture of CH_2Cl_2 and *n*-hexane (1:1 by volume) as the eluent.

(**G1**)$_3$**Ir**: Yellow solid. Yield = 80%. ^{1}H NMR ($CDCl_3$, 400 MHz, ppm): δ 7.64–7.55 (m, 9H), 7.47 (d, J = 8.0 Hz, 3H), 7.39 (d, J = 8.0 Hz, 3H), 7.21–7.15 (m, 15H), 7.02–6.96 (m, 6H), 6.76 (td, J = 8.4, 1.6 Hz, 3H), 6.51 (d, J = 8.4 Hz, 6H), 6.28 (d, J = 8.0 Hz, 3H), 6.14 (dd, J = 8.4, 1.6 Hz, 3H), 4.67 (d, J = 12.0 Hz, 3H), 4.62 (d, J = 12.0 Hz, 3H). FABMS: m/z 1319.3 ((M+H)$^+$). Anal. Calcd. for $C_{78}H_{57}N_6O_3Ir$: C, 71.05; H, 4.36; N, 6.37. Found: C, 70.70; H, 4.20; N, 6.43.

(**G2**)$_3$**Ir**: Yellow solid. Yield = 45%. ^{1}H NMR ($CDCl_3$, 400 MHz, ppm): δ 7.54–7.50 (m, 9H), 7.48 (d, J = 8.0 Hz, 3H), 7.40–7.35 (m, 3H), 7.29–7.23 (m, 30H), 7.08–6.96 (m, 6H), 6.76 (t, J = 8.4 Hz, 3H), 6.57 (d, J = 2.4 Hz, 3H), 6.51–6.42 (m, 9H), 6.42–6.37 (m, 6H), 6.11 (dd, J = 8.4, 1.6 Hz, 3H), 4.87 (m, 12H), 4.61 (d, J = 12.0 Hz, 3H), 4.57 (d, J = 12.0 Hz, 3H). FABMS: m/z 1954.9 (M$^+$). Anal. Calcd. for $C_{120}H_{93}N_6O_9Ir$: C, 73.71; H, 4.79; N, 4.30. Found: C, 73.68; H, 4.86; N, 4.26.

(**G3**)$_3$**Ir**: Yellow solid. Yield = 18%. ^{1}H NMR ($CDCl_3$, 400 MHz, ppm): δ 7.49–7.41 (m, 15H), 7.34–7.26 (m, 60H), 7.01–6.97(m, 6H), 6.89–6.80 (m, 6H), 6.66–6.57 (m, 12H), 6.57–6.52 (m, 6H), 6.52–6.48 (m, 6H), 6.48–6.45 (m, 6H), 6.45–6.41 (m, 6H), 5.06 (s, 12H), 4.96–4.93 (m, 12H), 4.79–4.77 (m, 12H), 4.66–4.63 (m, 6H). MADLI-TOF: m/z 3223.1(M$^+$). Anal. Calcd. for $C_{204}H_{165}N_6O_{21}Ir$: C, 75.89; H, 5.15; N, 2.60. Found: C 75.67, H 5.33, N 2.50.

4. Results and discussion

4.1. Synthesis of materials

The chemical structures of the synthesized iridium dendrimers (**G*n***)$_2$**Ir**(**acac**) and (**G*n***)$_3$**Ir** (***n*** = **0**, **1**, **2**, and **3**) are shown in Chart 1. The synthetic procedures of all dendritic ligands **G*n*** (***n*** = **0**–**3**) are illustrated in Scheme 1 The zero-generation compounds **G0** [13], (**G0**)$_2$**Ir**(**acac**) [13], and (**G0**)$_3$**Ir** [12] were reported in the literatures. The reaction of *N*-phenyl-*o*-phenylenediamine with 4-hydroxybenzaldehyde provided 2-(phenol-4-yl)-1-phenyl-1*H*-benzoimidazole (Scheme 1a), which further reacted with benzyl bromide dendrons (**D*n*–CBr**) (***n*** = **1**–**3**) in DMF at 100 °C to form dendritic ligands **G*n*** (Scheme 1b), where the benzyl bromide dendrons (**D*n*–CBr**) were prepared according to the procedure described by Fréchet and Hawker [15,16]. The synthetic procedures of iridium dendrimers (**G*n***)$_2$**Ir**(**acac**) and (**G*n***)$_3$**Ir** (***n*** = **1**–**3**) are illustrated in Scheme 2. The preparation of cyclometalated iridium dendrimers (**G*n***)$_2$**Ir**(**acac**) and (**G*n***)$_3$**Ir** involved a two-step synthesis. Firstly, $IrCl_3 \cdot nH_2O$ and dendritic ligands (**G0**–**G3**) were reacted to form a chloro-bridged dimer. The dimer

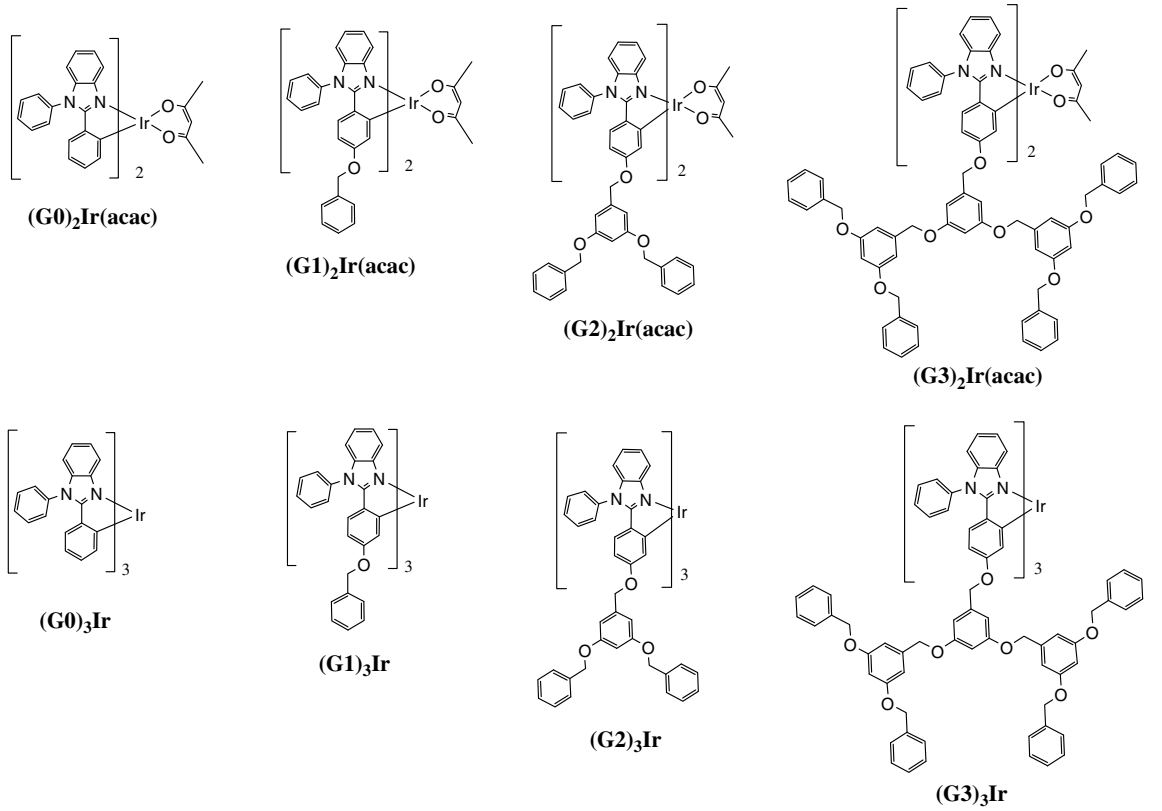

Chart 1. Chemical structures of iridium dendrimers (**G*n***)$_2$**Ir**(**acac**) and (**G*n***)$_3$**Ir** (***n*** = **0**–**3**).

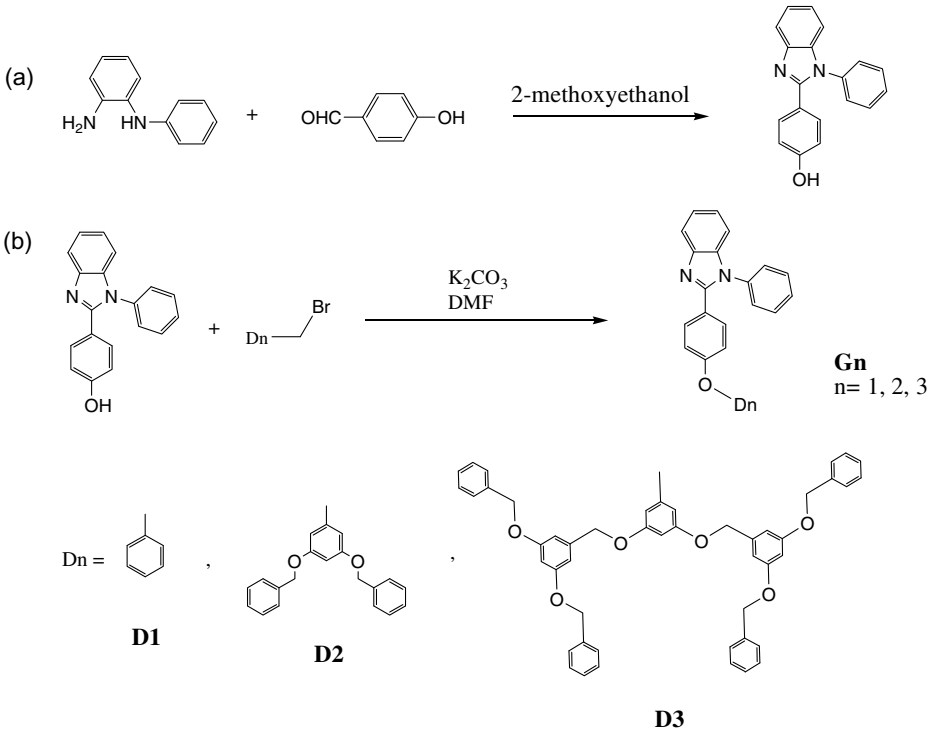

Scheme 1. Synthetic procedures of dendritic ligands **G*n*** (***n*** = **0–3**).

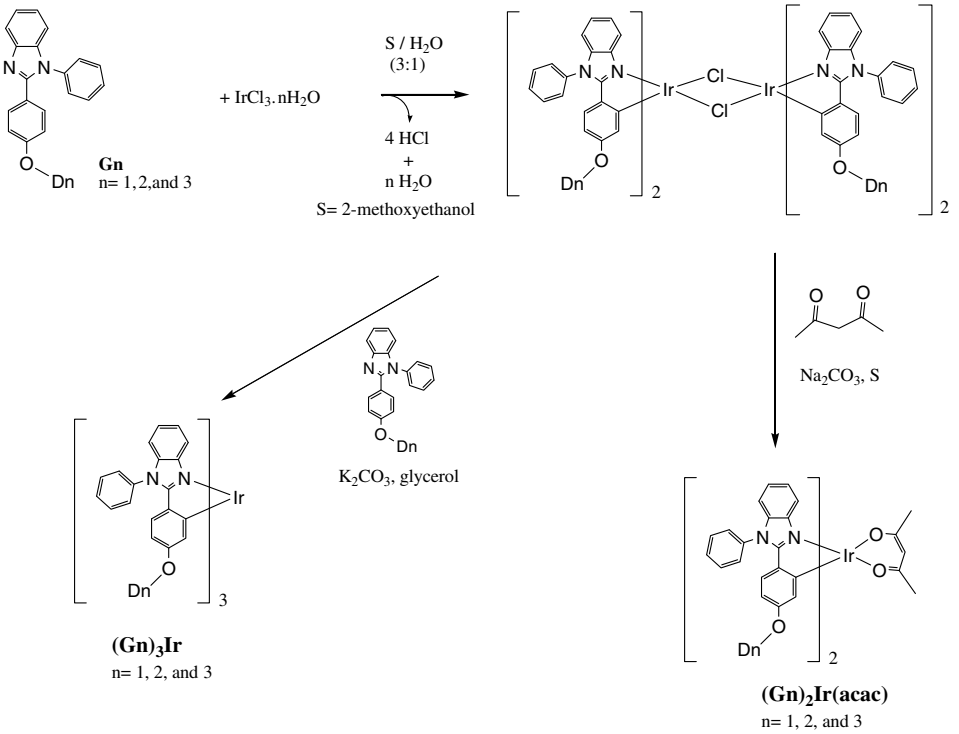

Scheme 2. Synthetic procedures of iridium dendrimers (**G*n***)$_2$**Ir**(**acac**) and (**G*n***)$_3$**Ir** (***n*** = **1–3**).

was then treated with 2,4-pentanedione in the presence of base to form (**G*n***)$_2$**Ir**(**acac**), or with additional **G*n*** in glycerol at 190 °C to give (**G*n***)$_3$**Ir**, where only facial (*fac*) isomers were obtained as evidenced from the NMR spectra.

4.2. Optical properties

The photophysical data of dendritic ligands **G*n*** and iridium dendrimers ((**G*n***)$_2$**Ir**(**acac**) and (**G*n***)$_3$**Ir**) are displayed in Table 1. Representative absorption spectra of dendritic ligands and iridium complexes are shown in Fig. 1. The ligands exhibit an absorption band at ~300 nm ($\varepsilon \sim 10^4$–10^5 M^{-1} cm^{-1}), which is characteristic of the π–π^* transition of benzoimidazolyl moieties [13]. The π–π^* transition of benzenoids from the dendrons appears as a prominent shoulder at ~285 nm for **G3**. All dendritic iridium complexes have similar absorption spectra. Besides the π–π^* transition bands of the ligands, they also exhibit weak absorption bands in the range of ~350–500 nm attributed to metal-to-ligand charge transfer transitions, i.e., ^{1}MLCT and ^{3}MLCT.

Ligands **G*n*** in CH_2Cl_2 emit light in the violet-purple region. In contrast, all dendritic iridium complexes emit green light in both toluene solutions and solid films with λ_{em} in the range of 510–530 nm. Fig. 2 shows the representative solution and neat-film photoluminescent (PL) spectra of the dendritic iridium compounds. The solution PL spectra of the iridium dendrimers resemble one another, so do the solid PL spectra. All iridium dendrimers in toluene solutions exhibit high PL quantum yields (Φ_{PL} = 0.45–0.80), indicating the efficient mixing of singlet and triplet

Table 1
Physical data of dendritic ligands **G*n*** (***n*** = **0**–**3**) and iridium dendrimers (**G*n***)$_2$**Ir**(**acac**) and (**G*n***)$_3$**Ir** (***n*** = **0**-**3**)

Compound	λ_{abs}[a] (log ε) (nm)	λ_{em} (nm)	Φ_{PL}[c] (%)	λ_{em}[d] (nm)	Φ_{PL} (film) (%)[e]	τ[f] (μs)	τ_r[g] (μs)
G0	294 (4.3)	360[a]					
G1	296 (4.4)	354[a]					
G2	296 (4.4)	354[a]					
G3	285 (4.4), 297 (4.4)	354[a]					
(**G0**)$_2$**Ir**(**acac**)[h]	300 (4.6), 314 (4.6), 348 (4.1), 387 (4.0), 415 (3.6), 459 (3.6)	523[b]	71	530	16	1.82	2.56
(**G1**)$_2$**Ir**(**acac**)	302 (4.6), 314 (4.6), 350 (4.1), 385 (4.0), 420 (3.6), 450 (3.6)	510[b]	70	530	16	1.0	1.43
(**G2**)$_2$**Ir**(**acac**)	305 (4.6), 316 (4.6), 372 (4.1), 404 (3.8), 429 (3.6)	510[b]	80	524	32	1.10	1.25
(**G3**)$_2$**Ir**(**acac**)	261 (4.8), 279 (4.8), 300 (4.6), 315 (4.6), 372 (4.1), 406 (3.8), 434 (3.6)	510[b]	68	513	41	1.13	1.66
(**G0**)$_3$**Ir**[i]	298 (4.6), 313 (4.6), 375 (4.1), 410 (3.8), 453 (3.5)	517[b]	45	534	15	1.07	2.37
(**G1**)$_3$**Ir**	299 (4.6), 312 (4.6), 376 (4.1), 385 (4.0), 411 (3.8), 454 (3.5)	523[b]	64	527	28	1.26	1.97
(**G2**)$_3$**Ir**	303 (4.6), 317 (4.6), 357 (4.1), 374 (4.1), 405 (3.8), 432 (3.5)	523[b]	65	524	40	1.11	1.71
(**G3**)$_3$**Ir**	278 (4.8), 299 (4.6), 313 (4.6), 351 (4.3), 408 (3.8), 428 (3.4)	523[b]	75	516	45	1.37	1.83

[a] Measured in CH_2Cl_2 10^{-5} M at 298 K. ε is the absorption coefficient.
[b] Recorded in toluene solutions at 298 K. Excitiaton wavelength was 410 nm for all iridium compounds.
[c] Quantum yield was measured with respect to **Ir**(**ppy**)$_3$ (Φ_p = 0.4 in toluene).
[d] Neat-film data measured at 298 K. Excitiaton wavelength was 350 nm.
[e] PL quantum efficiencies in film measured in an integrating sphere.
[f] Measured in toluene solutions at 298 K.
[g] $\tau_r = \tau/\Phi_p$.
[h] Ref. [13].
[i] Ref. [12].

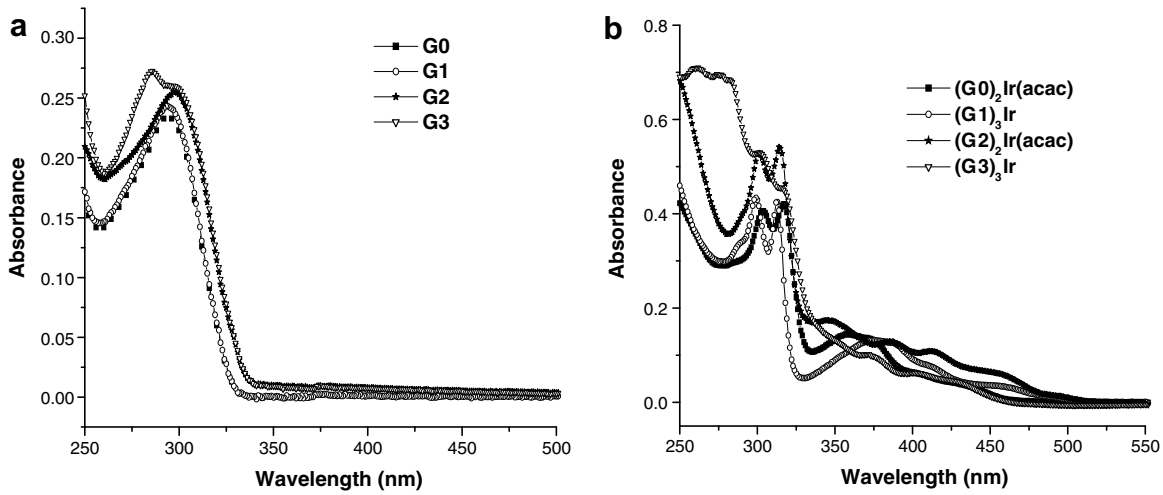

Fig. 1. Absorption spectra in CH_2Cl_2 solutions of (a) ligands **G*n***; (b) iridium dendrimers (**G*n***)$_2$**Ir**(**acac**) and (**G*n***)$_3$**Ir**.

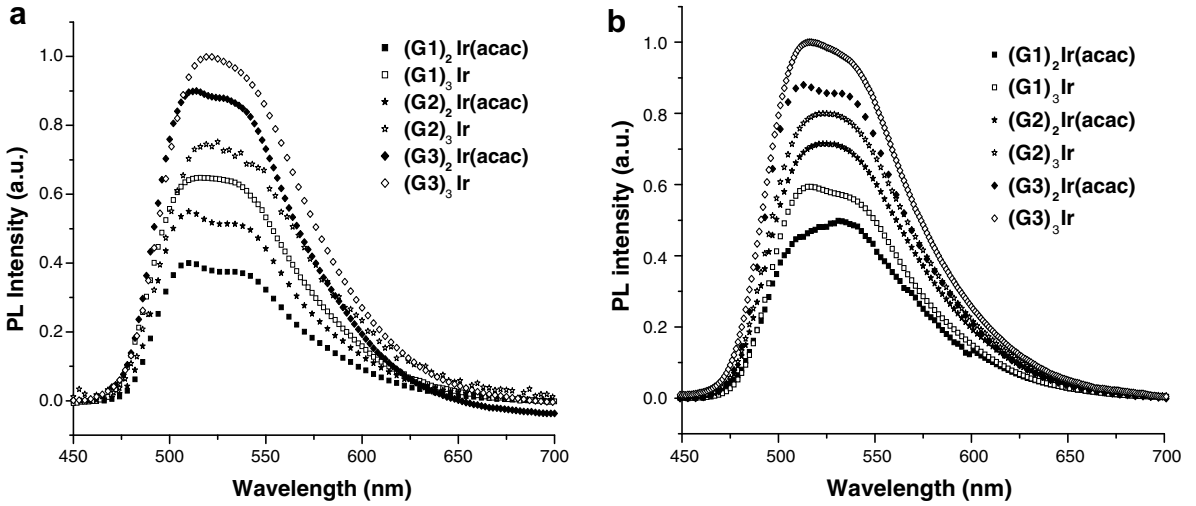

Fig. 2. PL spectra of iridium dendrimers in (a) toluene at 298 K; (b) solid films.

excited states via spin-orbit coupling. The PL quantum yields (Φ_{PL} = 0.16–0.45) in the solid films drop due to intermolecular interaction. In both the solution and solid films, the PL quantum yields increase as the dendrtric generation increases, indicating that there is less intermolecular interaction in higher generation dendrimers. The phosphorescence lifetime (τ = 1.25–1.97 μs) of these dendrimers in the solution fall in the same range as their non-dendronized congeners, i.e., (**G0**)$_2$**Ir**(**acac**) (τ = 1.82 μs) and (**G0**)$_3$**Ir** (τ = 1.07 μs).

4.3. Electrochemical studies

The electrochemical properties of these iridium dendrimers were studied by cyclic voltammetry (CV), and the electrochemical data are summarized in Table 1. A quasi-reversible one-electron oxidation wave attributed to the oxidation of iridium(III) was detected at ~550 mV for (**G*n***)$_2$**Ir**(**acac**)and ~370 mV for (**G*n***)$_3$**Ir** vs. Ag/AgNO$_3$, respectively. The dendrons in iridium complexes, (**G*n***)$_2$**Ir**(**acac**) and (**G*n***)$_3$**Ir**, appear to have negligible influence on the oxidation potentials of the iridium centers, possibly due to the non-conjugated nature of the spacers between the dendrons and the iridium centers. The energies of the highest occupied molecular orbitals (HOMOs) in (**G*n***)$_2$**Ir**(**acac**) and (**G*n***)$_3$**Ir** were calculated relative to ferrocene (Fc) which has a value of 4.8 eV with respect to the vacuum level [17]. The HOMO energies in combination with the optical band gaps derived from the absorption band edges were used to calculate the energies of the lowest unoccupied molecular orbitals (LUMOs) of the iridium dendrimers. Both HOMO and LUMO data are also collected in Table 2. No reduction waves up to −2.0 V were detected in these iridium dendrimers.

Table 2
Oxidation potentials and HOMO/LUMO energies of iridium dendrimers (**G*n***)$_2$**Ir**(**acac**) and (**G*n***$_3$)**Ir** (***n*** = **0–3**)

Compound	E_{ox} (ΔE_p) (mV)	HOMO (eV)	LUMO (eV)	Band gap (eV)
(**G0**)$_2$**Ir**(**acac**)	550 (81)	5.12	2.44	2.68
(**G1**)$_2$**Ir**(**acac**)	555 (70)	5.11	2.44	2.67
(**G2**)$_2$**Ir**(**acac**)	560 (72)	5.11	2.44	2.67
(**G3**)$_2$**Ir**(**acac**)	562 (53)	5.10	2.44	2.66
(**G0**)$_3$**Ir**	370 (76)	4.95	2.44	2.51
(**G1**)$_3$**Ir**	377 (80)	4.95	2.44	2.51
(**G2**)$_3$**Ir**	362 (76)	4.95	2.44	2.51
(**G3**)$_3$**Ir**	365 (102)	4.93	2.44	2.49

Oxidation potential reported is adjusted according to the potential of ferrocene ($E_{1/2}$ = 230 mV vs. Ag/AgNO$_3$) which was used as an internal reference. Conditions of cyclic voltammetric measurements: glassy carbon working electrode; Ag/AgNO$_3$ reference electrode. Scan rate: 100 mV/s. Electrolyte: tetrabutylammonium hexafluorophosphate. HOMO levels calculated from CV potentials using ferrocene as a standard [HOMO = 4.8 + ($E_{ox} - E_{Fc}$)]. LUMO levels were derived via eq. *Eg* = HOMO − LUMO, where *Eg* was obtained from the absorption spectra.

5. Morphology of spin-casting films

The spirit of this research is to fabricate DLEDs using spin-coating technique. Therefore, TEM and AFM were used to examine the morphology of the spin-casting films for these complexes alone or their blends with a host (PVK or CBP). Fig. 3a and b shows TEM images of the CBP and PVK solid films with a 20 wt% iridium dendrimer ((**G2**)$_3$**Ir**) dopant. Phase segregation was evident in the PVK film and the domains of the aggregate were on the scales of ~20–50 nm. Because of the larger electron-scattering cross section of the iridium atom than the carbon atom, the dark spots are likely the aggregates of the Ir complexes. In comparison, the CBP blend film appears to be more homogeneous without abrupt phase segregation. AFM studies on the films were also carried out for more direct surface topography. Fig. 3c and d shows the AFM images of the spin-coated films (~45 nm thick), obtained from a blend of CBP with various amounts of iridium dendrimer (**G2**)$_3$**Ir**, on plasma treated indium tin oxide (ITO) substrates. Both pure iridium dendrimer (**G2**)$_3$**Ir** and its CBP blends were found to be able to form thin films of good quality. In contrast, a spin-coated film from a blend of CBP

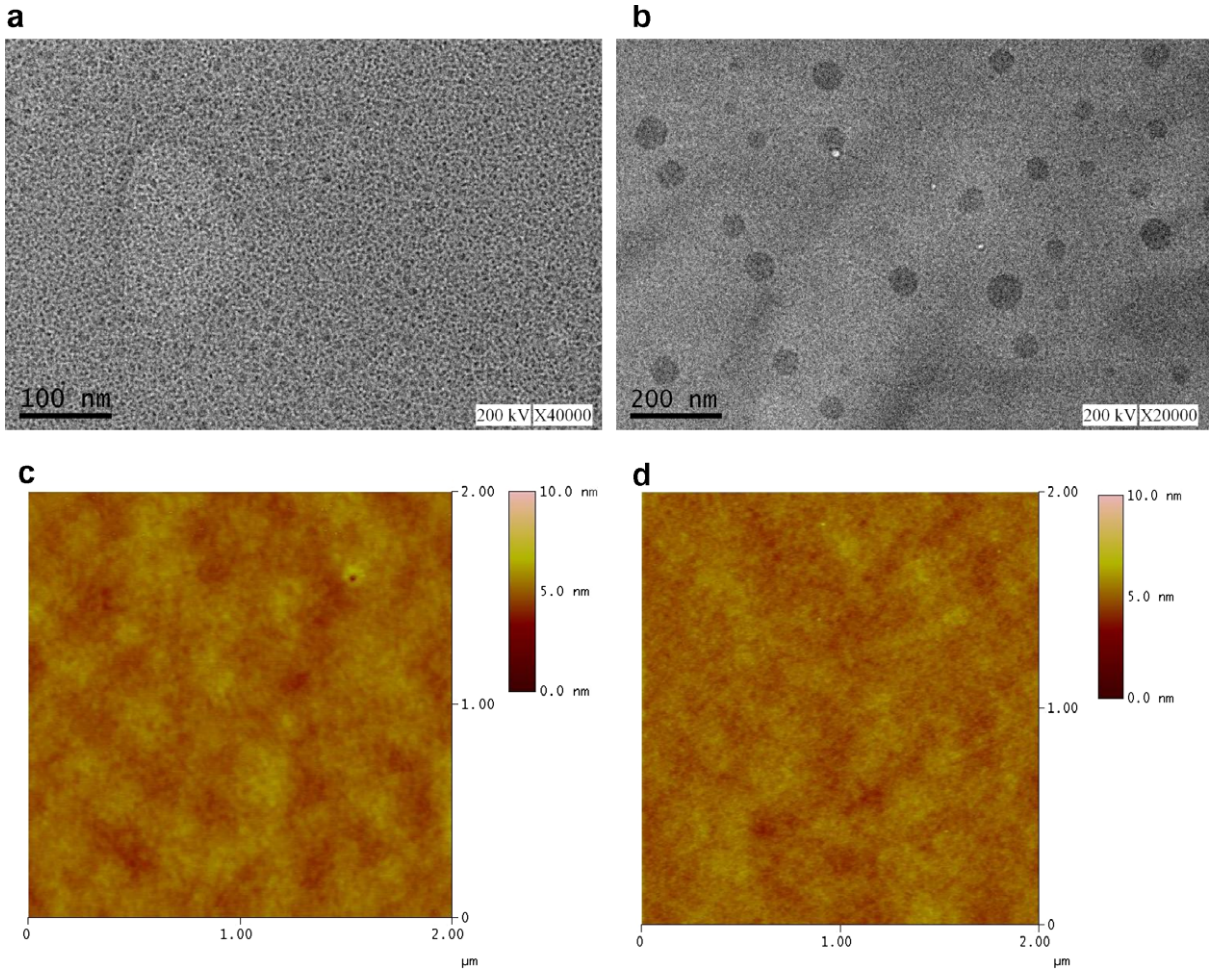

Fig. 3. TEM images of solid films of (a) 20 wt% (**G2**)$_3$**Ir** in CBP, (b) 20 wt% (**G2**)$_3$**Ir** in PVK and AFM images of solid films of (c) 20 wt% (**G2**)$_3$**Ir** in CBP, (d) pure (**G2**)$_3$**Ir**.

with 6 wt% of facial tris(2-phenylpyridine) iridium, (*fac*-**Ir**(**ppy**)$_3$), was reported to have a poor film quality [10b]. Both pure (**G2**)$_3$**Ir** film and the blend films of (**G2**)$_3$**Ir** (5–40 wt%):CBP have a similar root mean square (RMS) surface roughness of ~0.24 nm.

6. Electroluminescent (EL) properties

Because of the large triplet energy gaps, PVK (E_T = 2.5 eV) [18,19] and CBP (E_T = 2.56 eV) [20] are considered to be appropriate host for triplet green-emitters in this study. Sufficiently large triplet energy gap is essential for efficient exciton confinement inside the phosphorescent guest via energy transfer as well as suppression of back energy transfer from the triplet emitters to the host. The configurations of DLEDs using PVK and CBP as the host for the iridium dendrimers are shown in Fig. 4: (I) ITO/PEDOT:PSS (70 nm)/PVK:(**Gn**)$_3$**Ir** or (**Gn**)$_2$**Ir**(**acac**) (25–50 nm)/1,3,5-tris(*N*-phenylbenzimidazol-2-yl)benzene (TPBI) (40 nm)/LiF (1 nm)/Al (120 nm) and (II) ITO/PEDOT:PSS (70 nm)/CBP:(**Gn**)$_3$**Ir** or (**Gn**)$_2$**Ir**(**acac**) (30-70 nm)/TPBI (40 nm)/LiF (1 nm)/Al (120 nm). The structures of relevant compounds are also shown in Fig. 4, and the energy level alignments for the devices are shown in Fig. 5. Both types of the devices were fabricated by the spin-coating technique except that TPBI, the electron transporting and hole-blocking layer, was vacuum deposited. The performance parameters of DLEDs for both configurations are listed in Table 3. The representative EL spectra of devices I are shown in Fig. 6. For complete energy transfer from PVK to the iridium dendrimer, a higher mol% of the latter is needed as the dendrimer size grows larger. The better encapsulation of the emitting iridium center in the larger dendrimer apparently decreases the efficiency of the Förster energy transfer. Direction exciton formation [3c] on the dendrimer of larger generation is also expected to be less facile because of the non-conducting nature of peripheries. The best device efficiency of the devices I was found to be $\eta_{ext,max}$ = 8.6%, 9.7%, and 4.45%, and $\eta_{c,max}$ = 29.4, 32.5, and 15.3 cd/A for the DLED with 3.4, 4.6, and 6.9 mol% of (**G1**)$_3$**Ir**, (**G2**)$_3$**Ir** and (**G3**)$_3$**Ir**, respectively. The performances of devices I appeared to be inferior to those of device II, possibly due to serious phase segregation confirmed from TEM studies (vide supra).

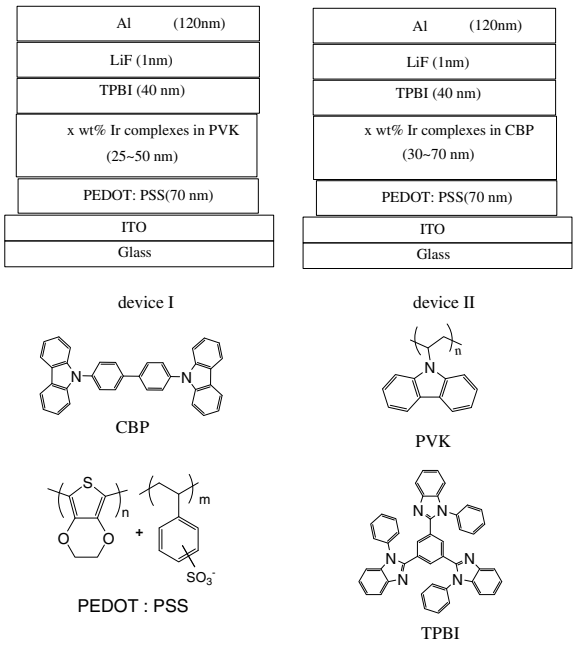

Fig. 4. The configurations of EL devices (i.e., devices I and II) and the molecular structures of the device compounds.

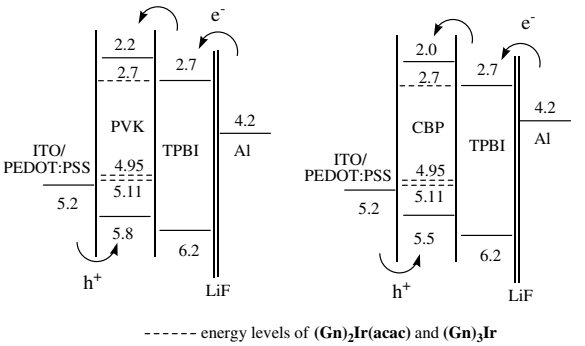

Fig. 5. Relative energy levels of the compounds utilized in the devices I and II.

Though CBP has a triplet energy gap similar to that of PVK, use of CBP is likely advantageous compared to PVK based on the following reasons: (1) the HOMO energy levels between CBP and PEDOT:PSS is smaller than those between PVK and PEDOT:PSS by ~0.3 eV and more facile hole injection from PEDOT:PSS into the host is expected. This may be beneficial to energy transfer from the host to the dendrimer; (2) CBP is ambipolar carrier-transporting [21] and better balance of charge carriers is expected in

Table 3
EL data of DLED devices with the configurations of devices I–II

Emitting layer	Brightness[a] (at V) (cd/m^2)	η_{ext}[a] (%)	η_c[a] (cd/A)	η_p[a] (lm/W)	V_{ON} (V)	λ_{em} (fwhm) (nm)	CIE at 12 V (x,y)
Device I							
PVK:(**G1**)$_3$**Ir** dopant 20 wt%	3239 (10.9);	4.8	16.2	4.6	3.5	522 (80)	0.32, 0.59
(3.38 mol%)	6061 (14.0);	1.8	6.0	1.3			
	6066 (14.5)	8.6	29.4	12.3			
PVK:(**G2**)$_3$**Ir** dopant 50 wt%	3485 (8.0);	5.2	17.5	6.8	3.5	522 (82)	0.32, 0.60
(4.56 mol%)	6046 (12.2);	1.8	6.0	1.5			
	6059 (12.5)	9.7	32.5	20.4			
PVK:(**G3**)$_3$**Ir** dopant 50 wt%	873 (12.7);	1.3	4.41	1.08	4.0	516 (74)	0.28, 0.61
(6.92 mol%)	683 (18.1);	0.20	0.68	0.12			
	996 (14.0)	4.5	15.3	6.90			
Device II							
CBP:(**G1**)$_3$**Ir** dopant 20 wt%	4540 (8.8);	6.5	22.8	8.1	3.5	522 (78)	0.31, 0.61
(7.36 mol%)	13661 (12.4);	3.9	13.7	3.5			
	22000 (16.5)	12.6	44.2	30.8			
CBP:(**G1**)$_3$**Ir** dopant 100 wt%	3355 (8.2);	5.0	17.0	6.6	3.0	528 (88)	0.33, 0.59
(36.8 mol%)	8468 (10.3);	2.6	8.6	2.6			
	11516 (7.6)	7.6	25.6	23.0			
CBP:(**G2**)$_3$**Ir** dopant 20 wt%	6213 (10.1);	8.9	31.2	9.7	3.0	518 (74)	0.29, 0.62
(4.92 mol%)	16923 (13.4);	4.9	17.0	4.0			
	20618 (15.5)	17.6	61.5	32.2			
CBP: (**G2**)$_3$**Ir** dopant 40 wt%	6213 (10.1);	10.4	30.5	9.6	3.5	518 (76)	0.29, 0.61
(9.84 mol%)	12912 (15.8);	4.4	13.0	2.7			
	13234 (17.5)	16.7	48.8	25.6			
CBP: (**G2**)$_3$**Ir** dopant 100 wt%	4617 (10.3);	6.8	23.4	7.1	3.0	524 (80)	0.31, 0.60
(24.6 mol%)	11556 (12.3);	3.4	11.7	3.0			
	12064 (13.0)	13.4	46.5	32.5			
CBP: (**G3**)$_3$**Ir** dopant 50 wt%	3279 (15.0);	5.2	16.4	3.4	7.5	510 (64)	0.24, 0.61
(7.5 mol%)	5551 (19.0);	1.8	5.6	0.9			
	5680 (18.0)	8.7	27.6	8.7			
CBP: (**G3**)$_3$**Ir** dopant 100 wt%	1876 (15.7);	2.7	9.5	1.9	9.5	528 (80)	0.30, 0.60
(15.0 mol%)	3833 (19.8);	1.1	3.8	0.7			
	3851 (20.0)	4.9	15.9	4.0			

[a] The first and second values were obtained at a current density of 20 mA and 100 mA, respectively. The third value is the maximum performance parameter of the device. fwhm, full width at half-maximum; η_{ext}, external quantum efficiency; η_c, current efficiency; η_p, power efficiency; V_{ON}, turn-on voltage, at a brightness of 1 cd/m^2.

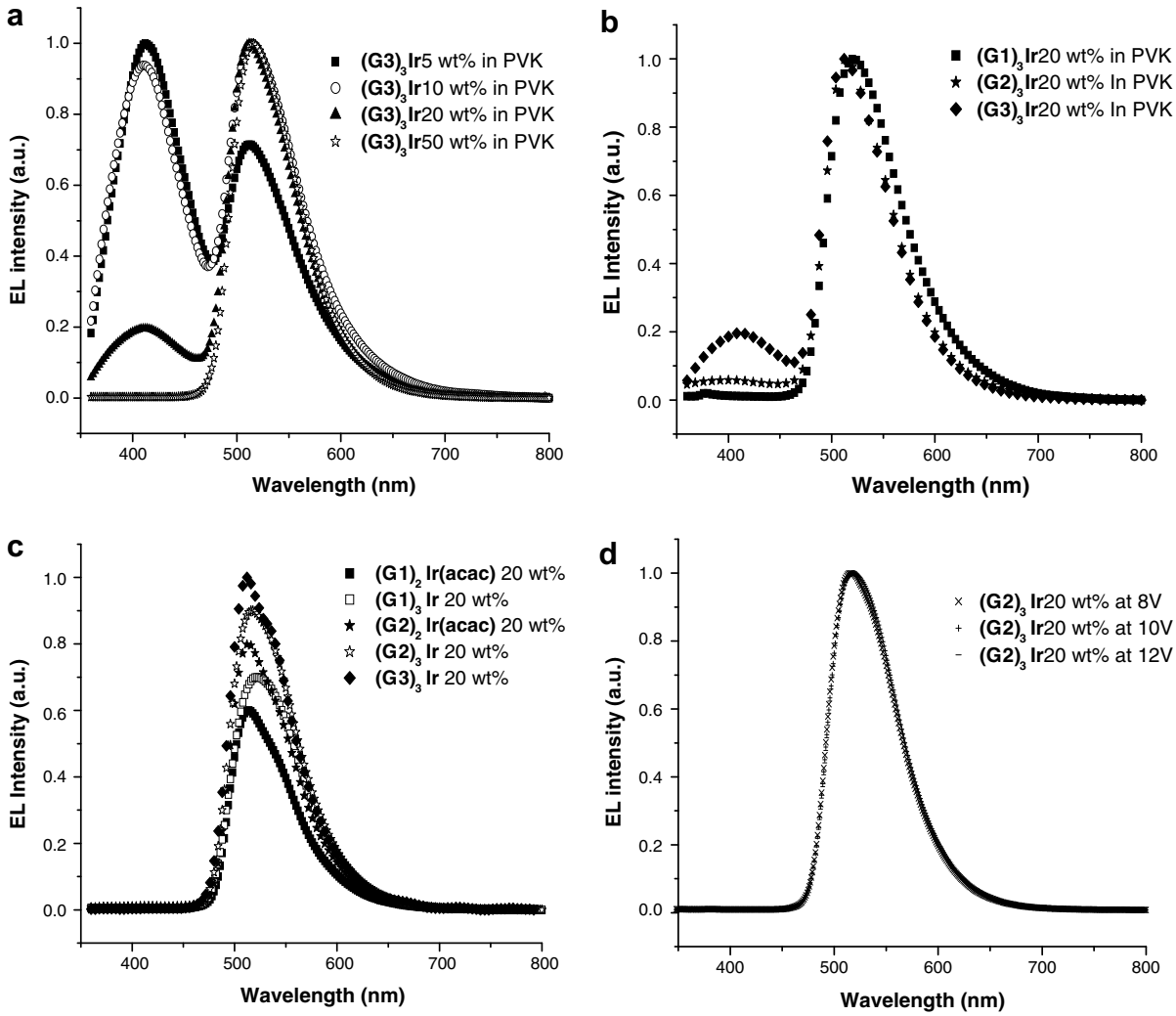

Fig. 6. (a) EL spectra of device II at a driving voltage of 12 V for various wt% of iridium dendrimer (**G3**)$_3$**Ir** in PVK; (b) EL spectra of device II at a driving voltage of 12 V for 20 wt% of various generations of iridium dendrimers (**G***n*)$_3$**Ir**in PVK; (c) EL spectra of device II at a driving voltage of 12 V for 20 wt% of various iridium dendrimers (**G***n*)$_3$**Ir** and (**G***n*)$_2$**Ir**(**acac**) in CBP; (d) EL spectra of device II at various driving voltages (8–12 V) for 20 wt% of iridium dendrimer (**G2**)$_3$**Ir** in CBP.

CBP compared to PVK which is a hole-only transporter; and (3) film from the blend of CBP and the dendrimers does not have noticeable phase segregation (vide supra). Indeed, CBP was reported to be a suitable host material for green-emitting **Ir**(**ppy**)$_3$, and the energy transfer from CBP to **Ir**(**ppy**)$_3$ was found to be efficient and the excitons were effectively confined inside **Ir**(**ppy**)$_3$ [22].

The representative EL spectra of devices II are shown in Fig. 6. Possibly due to inefficient encapsulation of emitting iridium core (the quantum yield in solid films: (**G***n*)$_2$**Ir**(**acac**) < (**G***n*)$_3$**Ir**), (**G***n*)$_2$**Ir**(**acac**)-based devices II exhibited efficiencies ($\eta_{ext,max}$ = 7.8–8.1% and $\eta_{c,max}$ = 26.8–27.7 cd/A) much inferior to those of (**G***n*)$_3$**Ir**-based devices. Therefore, only the performance of (**G***n*)$_3$**Ir**-based devices II will be discussed further. Selected current–voltage (*I*–*V*) characteristics and the external quantum efficiency and current efficiency vs. current density are shown in Figs. 7 and 8. Devices with optimal performances have dendrimers in a doping concentration of ~5.0–9.8 mol%, similar to the devices reported by Burn and co-workers [10b] using **IrppyD**:CBP blends (**IrppyD** is a dendrimer with a *fac*-tris(2-phenylpyridine) iridium core, a phenylene-based dendritic spacer, and 2-ethylhexyloxy surface groups). Selected efficiency data for the devices with the best performance are shown as follows: (1) (**G1**)$_3$**Ir**-doped device: $\eta_{ext,max}$ = 12.6%, $\eta_{c,max}$ = 44.2 cd/A, $\eta_{p,max}$ = 30.8 lm/W, and turn-on voltage (V_{ON}) = 4.0 V at 20 wt% (7.36 mol%) doping concentration; (2) (**G2**)$_3$**Ir**-doped device: $\eta_{ext,max}$ = 17.6%, $\eta_{c,max}$ = 61.7 cd/A, $\eta_{p,max}$ = 32.2 lm/w, and V_{ON} = 3.5 V at 20% (4.92 mol%) doping concentration; and (3) (**G3**)$_3$**Ir**-doped device: $\eta_{ext,max}$ = 8.7%, $\eta_{c,max}$ = 27.6 cd/A, $\eta_{p,max}$ = 8.7 lm/w, and V_{ON} = 7.5 V at 50 wt% (7.50 mol%) doping concentration. The EL performances for the device II are in order of (**G3**)$_3$**Ir** < (**G1**)$_3$**Ir** < (**G2**)$_3$**Ir**. The better EL performances of (**G2**)$_3$**Ir**-based devices than (**G1**)$_3$**Ir**-based devices may be attributed to the better encapsulation of the emitting

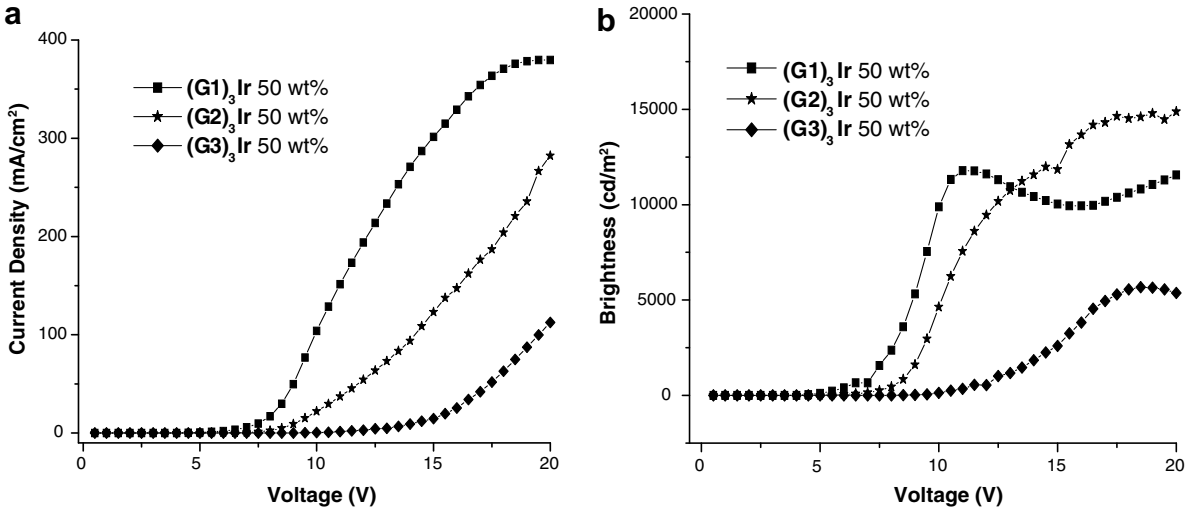

Fig. 7. EL characteristics of device II with 50 wt% of iridium dendrimers (**G*n***)$_3$**Ir** in CBP: (a) *I*–*V* plots; (b) *L*–*V* plots.

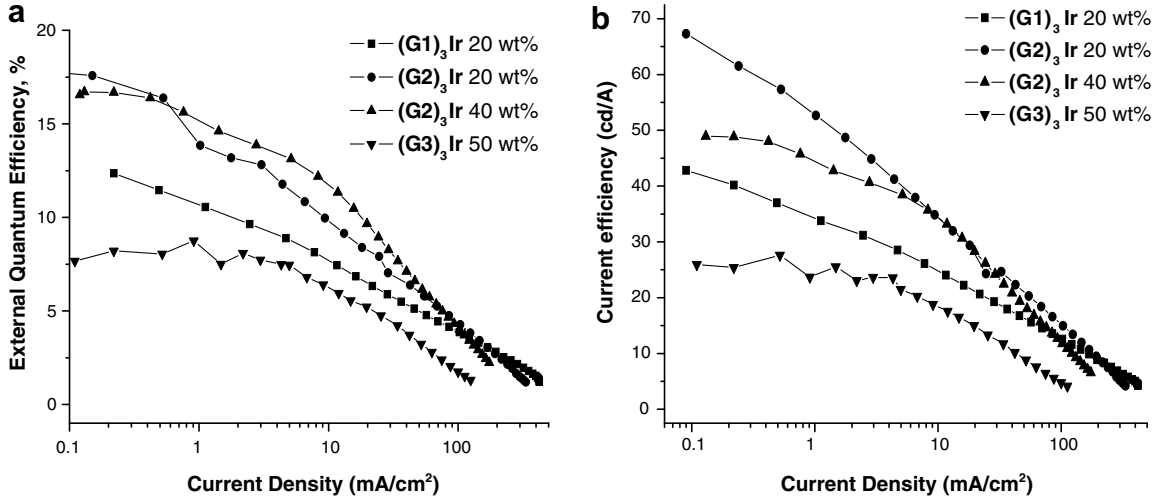

Fig. 8. EL properties of device II with selected dopant (iridium dendrimers) concentrations in CBP: (a) EQE vs. current density. (b) current efficiency vs. current density.

iridium center by the dendrons in the former. The merit of encapsulation by dendrons also reflects on suppressing the concentration quenching of the emission among (**G1**)$_3$**Ir**-based devices. As shown in Table 3, serious device deterioration occurred when the doping concentrations were increased to ca. 100 wt% for (**G1**)$_3$**Ir**-based devices II, e.g. $\eta_{ext,max}$ = 7.6% at 100 wt% of dopant concentration. In contrast, the efficiency of (**G2**)$_3$**Ir**-based devices II still retained high ($\eta_{ext,max}$ = 13.4%) even when the doping concentration was increased to around 100 wt%. Apparently, the core of iridium dendrimer (**G2**)$_3$**Ir** was better protected by the surrounding dendrons, and the intermolecular interaction and aggregation were more effectively suppressed. Though the iridium core in dendritic complex (**G3**)$_3$**Ir** was considered to have the best encapsulation by the dendrons, the EL performance of (**G3**)$_3$**Ir**-based devices was inferior to those of (**G1**)$_3$**Ir**- and (**G2**)$_3$**Ir**-based devices. In view of the larger turn-on voltage and lower current density found in (**G3**)$_3$**Ir**-based devices in Fig. 7, we speculate that the peripheral benzyl ether dendrons behave as insulating arms of the dendritic iridium emitter. Therefore, it is possible that the larger insulating peripheries of dendrons in (**G3**)$_3$**Ir** retard the transporting of electrons in the emitting layer and blockade the confinement of excitons in the emitting cores. Compared to the device I, the EL spectra of the device II fabricated from (**G*n***)$_2$**Ir**(**acac**) or (**G*n***)$_3$**Ir** were nearly superimposable with their film PL (Fig. 6c), indicating very efficient energy transfer from CBP to the iridium guest. Devices II containing iridium dendrimer (**G2**)$_3$**Ir** retained a very stable Commission Internationale de L'Eclairage (CIE) coordinate at an applied voltage ranging from 8 to 12 V (Fig. 6d). Therefore, CBP is more appropriate than PVK as

the host material for the green-emitting iridium dendrimers to be developed for highly efficient DLEDs in this study.

7. Conclusions

In summary, first-, second-, and third-generation of phosphorescent benzoimidazole-based iridium dendrimers containing peripheral benzyl ether dendrons were synthesized and characterized in this study. These iridium dendrimers emit green light and exhibit high solution quantum yields ranging from 0.45 to 0.80. The iridium dendrimers-based DLEDs fabricated by spin-coating technique exhibited promising EL performances. For highly efficient DLEDs based on green-emitting iridium dendrimers, CBP is more appropriate than PVK as the host material. The best efficiencies found in the DLEDs containing 20–50 wt% (4.5–9.8 mol%) of iridium dendrimers ($\mathbf{G}\boldsymbol{n})_3\mathbf{Ir}$ ($\boldsymbol{n}$ = **1**–**3**) doped in CBP host. Among these, the device with 20 wt% dopant has the best EL performance with a maximum EQE of 17.6% and a maximum current efficiency of 61.5 cd/A.

Acknowledgements

We thank the Academia Sinica, National Chiao Tung University and the National Science Council for supporting this work.

References

[1] C.W. Tang, S.A. Van Slyke, Appl. Phys. Lett. 51 (1987) 913.
[2] J.H. Burroughes, D.D.C. Bradley, A.R. Brown, R.N. Mackay, K. Marks, R.H. Friend, P.L. Burns, A.B. Holmes, Nature 347 (1990) 539.
[3] (a) M.A. Baldo, D.F. O'Brien, Y. You, A. Shoustikov, S. Sibley, M.E. Thompson, S.R. Forrest, Nature 395 (1998) 151;
(b) M.A. Baldo, D.F. O'Brien, M.E. Thompson, S.R. Forrest, Phys. Rev. B 60 (1999) 14422;
(c) C. Adachi, M.A. Baldo, M.E. Thompson, S.R. Forrest, J. Appl. Phys. 90 (2001) 5048.
[4] (a) H.Z. Xie, M.W. Liu, O.Y. Wang, X.H. Zhang, C.S. Lee, L.S. Hung, S.T. Lee, P.F. Teng, H.L. Kwong, H. Zheng, C. Che, Adv. Mater. 13 (2001) 1245;
(b) V.V. Grushin, N. Herron, D.D. LeCloux, W.J. Marshall, V.A. Petrov, Y. Wang, Chem. Commun. (2001) 1494;
(c) J. Ostrowski, M.R. Robinson, A.J. Heeger, G.C. Bazan, Chem. Commun. (2002) 784;
(d) J.-P. Duan, P.-P. Sun, C.-H. Cheng, Adv. Mater. 15 (2003) 24;
(e) Y.-J. Su, H.-L. Huang, C.-L. Li, C.-H. Chien, Y.-T. Tao, P.-T. Chou, S. Datta, R.-S. Liu, Adv. Mater. 15 (2003) 884;
(f) A.B. Tamayo, B.D. Alleyne, P.I. Djurovich, S. Lamansky, I. Tsyba, N.N. Ho, R. Bau, M.E. Thompson, J. Am. Chem. Soc. 125 (2003) 7377.
[5] (a) W. Lu, B.-X. Mi, M.C.W. Chan, Z. Hui, N. Zhu, S.-T. Lee, C.-M. Che, Chem. Commum. (2002) 206;
(b) B.W. D'Andrade, J. Brooks, V. Adamovich, M.E. Thompson, S.R. Forrest, Adv. Mater. 14 (2002) 1032.
[6] Y. Ma, H. Zhang, J. Shen, C.-M. Che, Synthetic Metals 94 (1998) 245.
[7] Y. Ma, C.-M. Che, H.-Y. Chao, X. Zhou, W.-H. Chan, J. Shen, Adv. Mater. 11 (1999) 852.
[8] (a) J.R. Carlise, X.-Y. Wang, M. Weck, Macromolecules 38 (2005) 9000;
(b) Y. You, S.H. Kim, H.K. Jung, S.Y. Park, Macromolecules 39 (2006) 349;
(c) C.L. Schulz, X. Chen, S.-A. Chen, S. Holdcroft, Macromolecules 39 (2006) 9157;
(d) H. Zhen, C. Luo, W. Yang, W. Song, B. Du, J. Jiang, C. Jiang, Y. Zhang, Y. Cao, Macromolecules 39 (2006) 1693;
(e) N.R. Evans, L.S. Devi, C.S.K. Mak, S.E. Watkins, S.I. Pascu, A. Köhler, R.H. Friend, C.K. Willans, A.B. Holms, J. Am. Chem. Soc. 128 (2006) 6647.
[9] (a) P.W. Wang, Y.J. Liu, C. Devadoss, P. Bharathi, J.S. Moore, Adv. Mater. 8 (1996) 237;
(b) M. Halim, J.N.G. Pillow, I.D.N. Samuel, P.L. Burn, Adv. Mater. 11 (1999) 371;
(c) A.W. Freeman, S.C. Koene, P.R.L. Malenfant, M.E. Thomson, J.M.J. Fréchet, J. Am. Chem. Soc. 122 (2000) 12385;
(d) A. Adronov, J.M.J. Fréchet, Chem. Commum. (2000) 1701;
(e) J.M. Lupton, I.D.W. Samuel, R. Beavington, M.J. Frampton, P.L. Burn, H. Bässler, Phys. Rev. B 63 (2001) 5206;
(f) C.-H. Chen, J.T. Lin, M.-C. Yeh, Org. Lett. 11 (2006) 2233.
[10] (a) T.D. Anthopoulos, M.J. Frampton, E.B. Namdas, P.L. Burn, I.D.W. Samuel, Adv. Mater. 16 (2004) 557;
(b) S.-C. Lo, N.A.H. Male, J.P.J. Markham, S.W. Magennis, P.L. Burn, I.D.W. Samuel, Adv. Mater. 14 (2002) 975;
(c) J.P.J. Markham, S.-C. Lo, S.W. Magennis, P.L. Burn, I.D.W. Samuel, Appl. Phy. Lett. 80 (2002) 2645;
(d) S.-C. Lo, G.J. Richard, J.P.J. Markham, E.B. Namdas, S. Sharma, P.L. Burn, I.D.W. Samuel, Adv. Funct. Mater. 15 (2005) 1451.
[11] S.-C. Lo, T.D. Anthopoulos, E.B. Namdas, P.L. Burn, I.D.W. Samuel, Adv. Mater. 17 (2005) 1945.
[12] J. Ding, J. Gao, Y. Cheng, Z. Xie, L. Wang, D. Ma, X. Jing, F. Wang, Adv. Funct. Mater. 16 (2006) 575.
[13] W.-S. Huang, J.T. Lin, C.-H. Chien, Y.-T. Tao, S.-S. Sun, T.-S. Wen, Chem. Mater. 16 (2004) 2480.
[14] A. Tsuboyama, H. Iwawaki, M. Furugori, T. Mukaide, J. Kamatani, S. Iawa, T. Moriyama, S. Miura, T. Takiguchi, S. Okada, M. Hoshino, K. Ueno, J. Am. Chem. Soc. 125 (2003) 12971.
[15] M. Kawa, J.M.J. Fréchet, Chem. Mater. 10 (1998) 286.
[16] C.J. Hawker, J.M.J. Fréchet, J. Am. Chem. Soc. 120 (1998) 286.
[17] J. Pommerehne, H. Vestweber, W. Guss, R.F. Mahrt, H. Bässler, M. Porsch, J. Daub, Adv. Mater. 7 (1995) 551.
[18] G. Rippen, G. Kaufmann, W. Klöpffer, Chem. Phys. 52 (1980) 152.
[19] (a) C.L. Lee, K.B. Lee, J.J. Kim, Appl. Phys. Lett. 77 (2000) 2280;
(b) S. Lamansky, R.C. Kwong, M. Nugent, P.I. Djurovich, M.E. Thompson, Org. Electron. 2 (2001) 53;
(c) Y. Kawamura, S. Yanagida, S.R. Forrest, J. Appl. Phys. 92 (2002) 87.
[20] (a) V.I. Adamovich, S.R. Cordero, P.I. Djurovich, A. Tamayo, M.E. Thompson, B.W. D'Andrade, S.R. Forrest, Org. Electron. 4 (2003) 77;
(b) K. Brunner, A.V. Dijken, H. Börner, J.J.A.M. Bastiaansen, N.M.M. Kiggen, B.M.W. Langeveld, J. Am. Chem. Soc. 126 (2004) 6035.
[21] H. Kanai, S. Ichinosawa, Y. Sato, Synthetic Metals 91 (1997) 195.
[22] M.A. Baldo, C. Adachi, S.R. Forrest, Phys. Rev. B 62 (2000) 10967.